Dynamics and pattern formation of ring dark solitons in a two-dimensional binary Bose-Einstein condensate with tunable interactions

Zhang-Ming He,[1] L. Wen,[2,*] Ya-Jun Wang,[3,4] G. P. Chen,[5] R.-B. Tan,[6] C.-Q. Dai,[7,†] and Xiao-Fei Zhang[3,4,‡]

[1]*College of Science, Hunan University of Technology, Zhuzhou 412007, China*

[2]*College of Physics and Electronic Engineering, Chongqing Normal University, Chongqing 400047, China*

[3]*Key Laboratory of Time and Frequency Primary Standards, National Time Service Center, Chinese Academy of Sciences, Xi'an 710600, China*

[4]*School of Astronomy and Space Science, University of Chinese Academy of Sciences, Beijing 100049, China*

[5]*School of Physics and Mechtronic Engineering, Sichuan University of Art and Science, Dazhou 635000, China*

[6]*College of Mathematics and Physics, Chongqing University of Science and Technology, Chongqing 401331, China*

[7]*School of Sciences, Zhejiang A&F University, Lin'an, Zhejiang 311300, China*

(Received 26 February 2019; revised manuscript received 20 May 2019; published 19 June 2019)

We investigate the dynamics and pattern formation of two ring dark solitons in a two-dimensional binary Bose-Einstein condensate with tunable intercomponent interaction via numerical simulation of the time-dependent Gross-Pitaevskii equation. Both the black and gray ring dark solitons are considered for cases where the modulation frequency of the intercomponent interaction is resonant or nonresonant with the one of the trapping potential. Our results show that in the presence of periodic modulation of the intercomponent interaction not only are the lifetimes of the ring dark solitons largely extended but also their decaying dynamics are dramatically affected. Before snaking instability sets in, new ring dark solitons are formed, and both the numbers and depths of the ring dark solitons exhibit collective oscillations. With the development of instability, the system exhibits different decaying processes, and a variety of decay profiles, such as vortex necklace, distorted octagon, vortex-antivortex ring, and cross, are formed, showing a strong dependence on the modulation frequency of the intercomponent interaction and the initial depth of the ring dark soliton.

DOI: 10.1103/PhysRevE.99.062216

I. INTRODUCTION

Since the experimental realization of multicomponent Bose-Einstein condensates (BECs), the ground states, dynamics, and various nonlinear excitations that arise in them have been a focal research over the past two decades [1–10]. Compared with the single-component BEC (which is also called the scalar condensate), the extra internal degrees of freedom introduced by multicomponent BECs give rise to more rich nonlinear excitations and complex dynamical behaviors, such as a variety of vector solitons, multidomain walls, self-bound three-dimensional solitons, and self-trapped quantum balls [11–20]. Among these nonlinear excitations, the ring dark soliton (RDS), which was first introduced in nonlinear optics [21–23], has been studied intensively and attracted more and more interest in both nonlinear optics and ultracold atom systems.

Within the zero-temperature mean-field theory, the static and dynamical properties of a binary BEC are well described by a system of coupled Gross-Pitaevskii (GP) equations, which is a variant of the well-known defocusing (repulsive contact interaction) or focusing (attractive contact interaction) vector nonlinear Schrödinger equations in nonlinear optics. Given their similar theory description and the versatility of ultracold atom systems, BECs offer us additional layers of tunability, enabling the study of dynamics of RDSs under a variety of parametric modulations [24–31]. Very recently, we have investigated the dynamics of vortices followed by the collapse of ring dark solitons in a two-component BEC, and found that the system exhibits complicated dynamical behaviors depending on the initial depths [32]. However, as far as we know, there has been little work on the effects of tunable contact interaction, which can be achieved in current experimental settings with the aid of Feshbach resonance management (FRM) [33–36], on the dynamical properties of RDSs in a binary BEC.

To fill up this gap, the aim of this paper is to bring to bear the enhanced understanding of the effects of tunable contact interactions on the dynamics of the RDSs in a two-dimensional (2D) binary BEC. More specifically, we will examine how the dynamics of the system is modified upon a periodic modulation of the intercomponent interaction. We start from the time-dependent version of the coupled GP equations, and preform a detailed study of the dynamics of RDSs by numerical simulations of such coupled equations. Here we want to note that in the presence of periodically modulated interaction, if the excited modes become largely populated, the contribution of the interactions from the excited modes must be taken into account to correct the time evolution of the GP equation and the corresponding Bogoliubov equations, which can be done by using the time-dependent Hartree-Fock

*wlqx@cqnu.edu.cn
†dcq424@126.com
‡xfzhang@ntsc.ac.cn

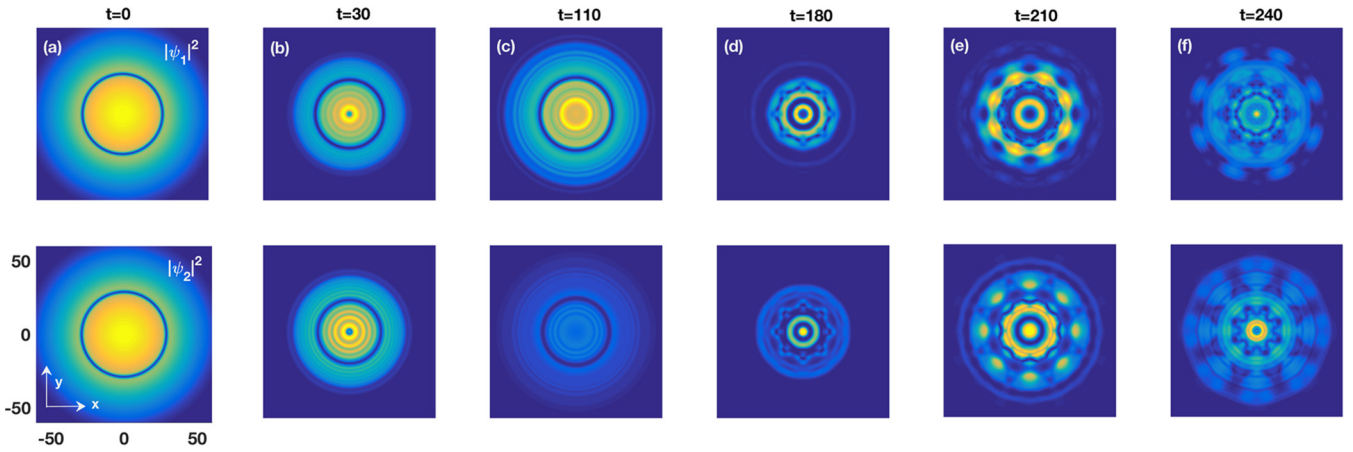

FIG. 1. The time evolutions of two black RDSs with resonant modulation frequency of the intercomponent interaction $\omega = 0.028$ for $t =$ (a) 0, (b) 30, (c) 110, (d) 180, (e) 210, and (f) 240, where the top row is for component 1 and the bottom one is for component 2. The initial depths of two such black RDSs $\cos\phi_1(0) = \cos\phi_2(0) = 1$, the initial locations $R_{10} = 27.9$ and $R_{20} = 28.9$, eccentricity $e_c = 0$, and the harmonic trap frequency $\Omega = 0.028$.

Bogoliubov theory [37,38]. Our main conclusion here is that, compared with the case with unvaried contact interaction, the tunable intercomponent interaction not only stabilizes and greatly extends the life of the RDSs [39,40] but also dramatically affects their dynamics.

This paper is organized as follows. In Sec. II, we introduce the theoretical model describing the RDSs in a quasi-two-dimensional (Q2D) binary BEC with tunable interactions, and briefly introduce the numerical method. The effects of tunable interactions on the dynamics and pattern formation of RDSs are investigated by using the mean-field theory in Sec. III. Finally, the main results are summarized in Sec. IV.

II. FORMULATION OF THE PROBLEM

We begin with the model describing a binary BEC trapped by a harmonic potential. Within the framework of zero-temperature mean-field theory, where the quantum and thermal fluctuations are negligible, the evolution of the system is governed by the following coupled GP equations:

$$\begin{aligned} i\hbar\frac{\partial\psi_1}{\partial t} &= \left(-\frac{\hbar^2\nabla^2}{2m_1} + V_{\rm ext}^1 + \beta_{11}|\psi_1|^2 + \beta_{12}|\psi_2|^2\right)\psi_1, \\ i\hbar\frac{\partial\psi_2}{\partial t} &= \left(-\frac{\hbar^2\nabla^2}{2m_2} + V_{\rm ext}^2 + \beta_{22}|\psi_2|^2 + \beta_{21}|\psi_1|^2\right)\psi_2, \end{aligned} \tag{1}$$

where the condensate wave functions are normalized as $N_i = \int(|\psi_i|^2)d\mathbf{r}dz$ with ψ_i being the wave function of the ith component, and m_i is the atom mass. $\beta_{ii} = 4\pi a_{ii}\hbar^2/m_i$ and $\beta_{ij} = 2\pi a_{ij}\hbar^2/m_R$ [$m_R = m_1m_2/(m_1+m_2)$ is the reduced mass] are the strengths of intra- and intercomponent interactions with a_{ii} and a_{ij} being the corresponding s-wave scattering lengths. In what follows, we assume that two components have the same mass $m_1 = m_2 = m$ and the condensed atoms are trapped in a very thin disk-shaped potential, i.e., the trapping potential in the radial direction (x-y plane) is much weaker than that in the axial (z) direction, such that the motion of atoms in the axial direction is essentially frozen to the ground state of the axial harmonic trapping potential. In this case, the external trapping potential is given by $V_{\rm ext}^i(r) = m\omega_r^2r^2/2$, where $r^2 = x^2 + y^2$ and ω_r denotes the confinement frequencies in the radial directions. After integrating out the axial coordinates, we obtain the following Q2D dimensionless equations for the radial parts of the wave functions [17,26,32,41]:

$$\begin{aligned} i\frac{\partial\psi_1}{\partial t} &= \left(-\frac{1}{2}\nabla^2 + g_{11}|\psi_1|^2 + g_{12}|\psi_2|^2 + \frac{1}{2}\Omega^2r^2\right)\psi_1, \\ i\frac{\partial\psi_2}{\partial t} &= \left(-\frac{1}{2}\nabla^2 + g_{22}|\psi_2|^2 + g_{21}|\psi_1|^2 + \frac{1}{2}\Omega^2r^2\right)\psi_2, \end{aligned} \tag{2}$$

where the effectively 2D contactlike interactions become $g_{ii} = \beta_{ii}/(\sqrt{2\pi}a_z)$ and $g_{ij} = \beta_{ij}/(\sqrt{2\pi}a_z)$, which can be attributed to the compression along the z axis. The aspect ratio of the trapping potential $\Omega = \omega_r/\omega_z$; $a_z = \sqrt{\hbar/m\omega_z}$ and $1/\omega_z$ are chosen as the units for length and time, respectively.

As is well known, it is not an easy question to deal with the tunable system parameters, especially the periodic modulation of the intercomponent interaction, which is also the nonlinear term in the Gross-Pitaevskii equation, since the decay of such solitons in a conventional condensate is very fast. We numerically propagate Eq. (2) by both the alternating-direction implicit method and the time-splitting Fourier spectral method, and the obtained results are cross checked and agree well with each other [42–44]. For the imaginary-time propagation, on the left-hand side of Eq. (2), i is replaced with -1. The numerical space is taken to be 300×300, which is sufficiently large, and the periodic boundary condition is used.

We start with a reasonable ansatz for the RDS with large initial radii [21,24]:

$$\psi_i(x, y, 0) = \left(1 - \frac{\Omega^2r^2}{4}\right)[\cos\phi_i(0)\tanh Z(r_1) + i\sin\phi_i(0)], \tag{3}$$

where $\cos\phi_i(0)$ denotes the depth of the input RDSs and $Z(r_1) = (r_1 - R_{i0})\cos\phi_i(0)$ with $r_1 = \sqrt{(1-e_c^2)x^2 + y^2}$ and e_c being the eccentricity of the ring. We note that $\cos\phi_i(0) \neq 1$ and $\cos\phi_i(0) = 1$ are corresponding to the oscillating gray and stationary black RDSs in the case with fixed contact interactions, respectively. In addition, $\triangle R = R_{20} - R_{10}$ represents

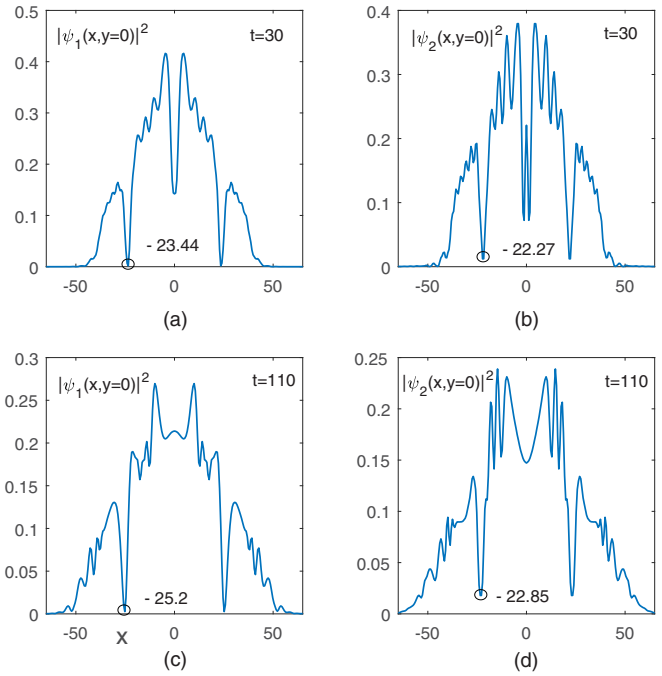

FIG. 2. The 1D density distributions at $t = 30$ (a, b) and at $t = 110$ (c, d) for the two-component system, corresponding to Figs. 1(b) and 1(c), respectively. Parameters are chosen as the same as those in Fig. 1.

the radius difference, which we set to be $\triangle R = 1$ throughout this paper.

To highlight the effects of intercomponent contact interaction, we further fix the intracomponent interactions as $g_{11} = g_{22} = 1$, which is most closely relevant to the ^{85}Rb system. In what follows we assume that the intercomponent interaction is varying periodically with time, which can be achieved through a small sinusoidal modulation of the magnetic field close to the Feshbach resonance. In this case, the intercomponent interaction can be written as

$$g_{12}(t) = 1 - m\sin(\omega t), \tag{4}$$

where ω is the modulation frequency and the amplitude m of the ac drive is small and satisfies $0 \leqslant m \leqslant 1$, leading to the modulation period $2\pi/\omega$. In this paper, we set $m = 1$, which keeps the mainly physical picture unchanged.

In real experiments, the most promising binary system can be realized by selecting $|F = 1, m_f = -1\rangle$ and $|2, 1\rangle$ spin states of ^{85}Rb. The system contains about 2×10^4 atoms, and is confined by a disk-shaped trap with radial frequency $\omega_\perp = 2\pi \times 18$ Hz and axial frequency $\omega_z = 2\pi \times 628$ Hz [6,26,45]. Therefore, the units of time and length are 0.25 ms and 0.42 μm, respectively, and the aspect ratio of the harmonic potential is $\Omega = 0.028$. Furthermore, the initially different RDS states Eq. (3) can be realized by imprinting different phases on two such components through far-off resonant laser pulses [27,46].

III. RESULTS AND DISCUSSION

In this section, we will perform a detailed numerical study of the dynamics of two RDSs in the presence of periodic modulation of the intercomponent interaction. We define the lifetime of the RDS as the time interval between the start and the time point when snaking instability sets in [26]. We note that there is no snake instability in an untrapped uniform BEC. However, in real ultracold atom experiments, the atomic gas is always trapped by an external potential, and consequently the snake instability is caused by the binding trap. In the presence of dipolar interaction, the trap in one direction can be removed and one can have a dark soliton in this system without snake instability [47].

It is well known that for a scalar system a deep RDS [typically with $\cos\phi_i(0) > 0.67$] can survive for only a short time before changing into other types of soliton. The RDS will suffer from the snaking instability, and in this case the FRM is believed to be a key factor for a long-lived RDS. Using the initial condition modeled in Eq. (3) with circular symmetry, i.e., $e_c = 0$, our numerical results show that the lifetimes of both black and gray RDSs can be largely extended, and their subsequent evolutions exhibit complicated decay dynamics.

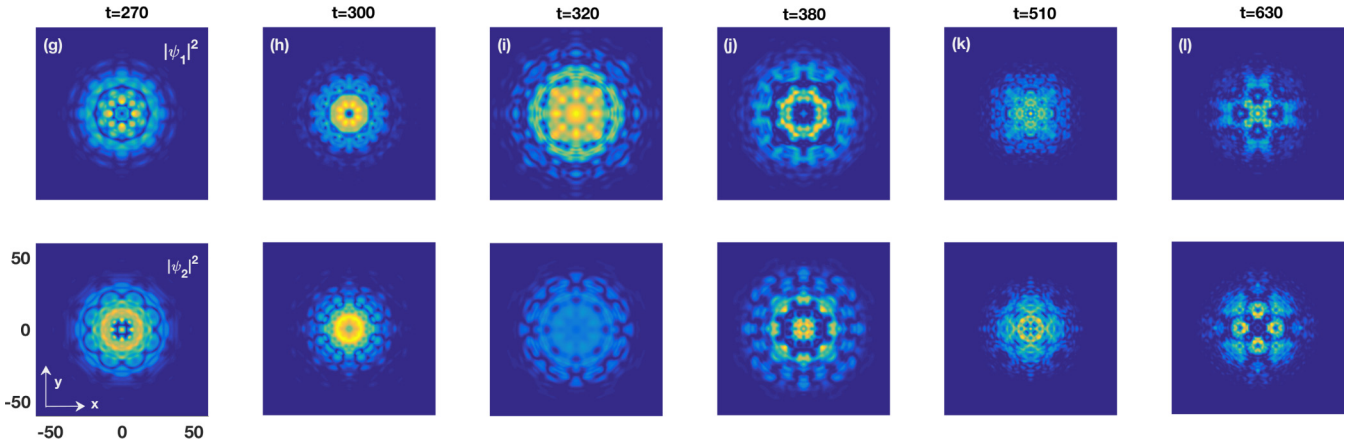

FIG. 3. The time evolutions of the system following Fig. 1 for $t =$ (g) 270, (h) 300, (i) 320, (j) 380, (k) 510, and (l) 630. Parameters are chosen as the same as those in Fig. 1.

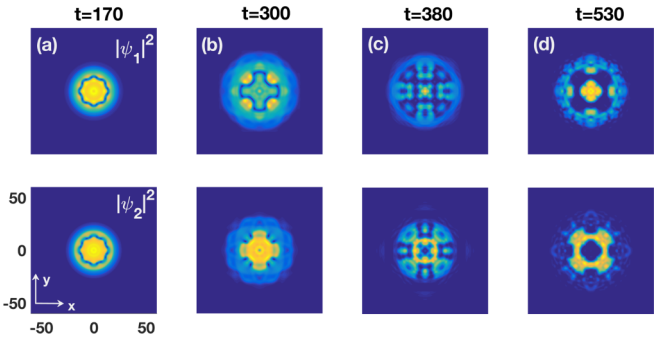

FIG. 4. The time evolutions of two black RDSs for $t =$ (a) 170, (b) 300, (c) 380, and (d) 530, where the top row is for component 1 and the bottom one is for component 2. The modulation frequency of the intercomponent interaction $\omega = 0.01$. Other parameters are the same as those in Fig. 1.

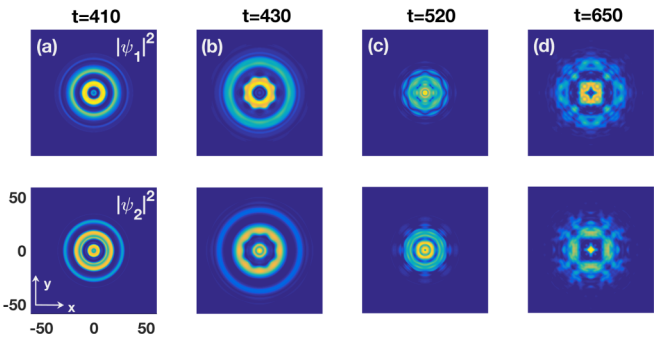

FIG. 6. The time evolutions of two deep gray RDSs for $t =$ (a) 410, (b) 430, (c) 520, and (d) 650, where the top row is for component 1 and the bottom one is for component 2. The initial depths of two such RDSs $\cos\phi_1(0) = \cos\phi_2(0) = 0.67$, and the modulation frequency of the intercomponent interaction $\omega = 0.028$. Other parameters are the same as those in Fig. 1.

A. Two black RDSs with periodic intercomponent interaction

We begin with two black RDSs, viz., $\cos\phi_1(0) = \cos\phi_2(0) = 1$, and consider the case where the modulation frequency of the intercomponent interaction is resonant with the one of the trapping potential. Figure 1 shows the time evolutions of two black RDSs with trapping potential $\Omega = 0.028$ and initial radius difference $\triangle R = 1$, where the first row is for component 1 and the bottom row is for component 2. Similar to the scalar system, in the presence of periodic modulation of the intercomponent interaction, the two black RDSs oscillate up to a certain time until instabilities develop [as shown in Fig. 1(d) for $t = 180$] [24,26]. During this process, new shallower RDSs (also called gray RDSs) appear and form a series of concentrically annular RDSs, as shown in Fig. 1(b) for $t = 30$, where the black RDSs are moving inward and several gray RDSs are formed. In addition, the numbers and depths of both newly formed shallow RDSs and the black one also exhibit oscillation behavior, which can be easily seen from the comparison between Figs. 1(b) and 1(c). We recall that for a scalar or spin-1 condensate with the absence of the $m = 0$ component system the location of the RDS exhibits roughly periodic oscillation [24,27,48]. In the presence of periodic modulation of the intercomponent interaction, the two-component system considered here also performs oscillation, but the roughly periodic one does not.

To give a clear description of the generic scenarios, the corresponding one-dimensional (1D) density distributions of $|\psi_i(x, y = 0)|^2$ are presented in Fig. 2. We take component 1 as an example, the location of the black RDS of which is -23.44 at $t = 30$ and -25.2 at $t = 110$, indicating that the black RDS first moves inward and then moves outward. In addition, the number and depths of all the RDSs exhibit oscillation behavior if we count the number of notches in the continuous background.

With increasing time, the snake instability sets in and one of the outer gray RDSs becomes distorted, and develops from a circle into an octagon, accompanied by a black RDS near the trap center. We note that the current system satisfies the widely accepted condition for phase separation, which is based on the consideration of minimizing the interaction energy [49,50]. In this case, the system shows phase separation, with the structure of a lump of component 2 surrounded by an annular concave of component 1. Typical density distribution of such a case is shown in Fig. 1(d) for $t = 180$. After a short interval,

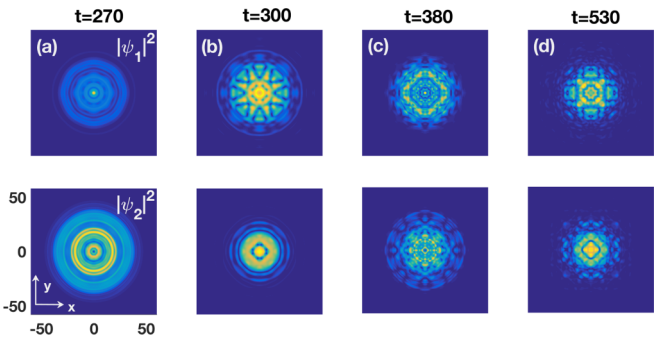

FIG. 5. The time evolutions of two black RDSs for $t =$ (a) 270, (b) 300, (c) 380, and (d) 530, where the top row is for component 1 and the bottom one is for component 2. The modulation frequency of the intercomponent interaction $\omega = 0.05$. Other parameters are the same as those in Fig. 1.

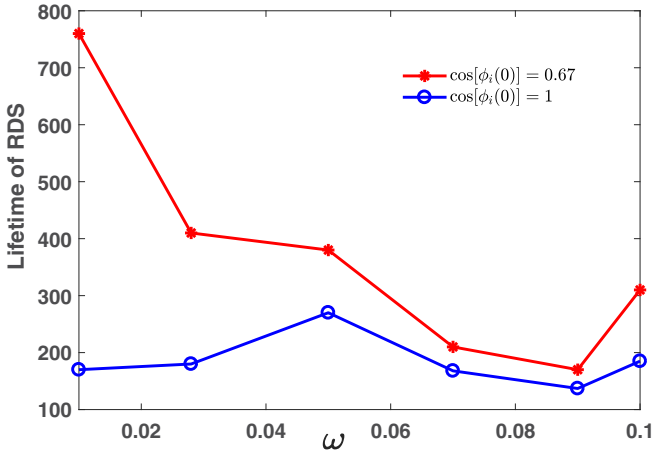

FIG. 7. The dependence of the lifetime of both black (blue line) and deep gray RDSs (red line) on the modulation frequency.

a vortex necklace consisting of eight visible vortices is formed at the outer edge of component 2, while eight notches are formed for component 1, as shown in Fig. 1(e) for $t = 210$. Later, the distorted RDSs continue to perform collective oscillations. It is interesting to notice that eight vortex-antivortex pairs appear in component 1, forming a ring structure, while the eight visible vortices in component 2 move inward and form a combined structure with the distorted RDS, as shown in Fig. 1(f) for $t = 240$.

Figure 3 shows the following decay dynamics of the system. Because of the continuous oscillation of the vortex necklace and the distorted RDS, a variety of exotic patterns are formed, as shown in Figs. 3(g) and 3(h) for $t = 270$ and 300, respectively. In addition, at $t = 300$ the distorted RDS begins to split and four fragments are formed. This phenomenon becomes more prominent over time, as shown in Fig. 3(i) for $t = 320$, where more fragments are formed and no visible RDS exists. After that, a variety of regular phase separation patterns are formed for different evolution times, as shown in Figs. 3(j)–3(l) for $t = 380$, 510, and 630, respectively.

Next we consider the case where the modulation frequency of the intercomponent interaction is not resonant with the one of the trapping potential. Figures 4 and 5 show the time evolutions of two black RDSs with modulation frequencies of the intercomponent interaction $\omega = 0.01$ and 0.05, respectively. Compared with the resonant case, the dynamics of the present systems before instabilities develop shows similar behavior with the previously resonant case, but the lifetimes of RDSs are obviously changed for different modulation frequencies, as shown in Figs. 4(a) and 5(a). For a small modulation frequency, such as $\omega = 0.01$ shown in Fig. 4(a), the snaking instability sets in at about $t = 170$, where regular octagons are formed in both components 1 and 2, while for a larger modulation frequency $\omega = 0.05$, shown in Fig. 5(a), this time point is about at $t = 270$, where a vortex necklace consisting of eight visible vortices is formed.

Figures 4(b)–4(d) and 5(b)–5(d) show the following decay dynamics of the system, during which different decay profiles are formed. It is interesting to see that the decaying process and the following decay profiles depend strongly on the modulation frequency of the intercomponent interaction. More specifically, at $t = 300$, a cross is formed for small modulation frequency $\omega = 0.01$ while eight sided petals are formed for large modulation frequency $\omega = 0.05$, as shown in Figs. 4(b) and 5(b), respectively. With increasing time, the system also exhibits a variety of regular phase separation patterns because the phase separation condition is always satisfied throughout the whole process.

B. Two deep gray RDSs with periodic intercomponent interaction

We now turn our attention to the dynamics of two deep gray RDSs. Our numerical results show that although the early-time dynamics of the present system is similar to the cases of black RDSs with different modulation frequencies the lifetimes of two gray RDSs are greatly extended compared with the black RDSs. A typical example is shown in Fig. 6 for two deep gray RDSs with initial depths $\cos\phi_1(0) = \cos\phi_2(0) = 0.67$ and modulation frequency of the intercomponent interaction $\omega = 0.028$. As shown in Fig. 6(a), the snake instability sets in at $t = 410$, which is much longer than any lifetimes of the black RDSs. Actually, as discussed before, a shallow RDS with strict circular symmetry will slowly decay into radiation, while snake instability sets in for a deep one [24]. For the two RDSs considered here, the instability increases with the increase of depth, and the deeper the depth the earlier the instabilities set in.

Figures 6(b)–6(d) show the following decay dynamics of the system, where we again find a composite structure consisting of a distorted RDS and a vortex necklace. A typical density profile of such a case is shown in Fig. 6(b) for $t = 430$. After that, the vortex necklace and the distorted RDS collectively maintain oscillation until they escape from the condensate, as shown in Fig. 6(c) for $t = 520$. This implies that the present distorted RDSs can exist for a longer time compared with case of initially black RDSs. With the development of instability, the long-time dynamics of the system shows similar behavior with the previous one, during which a variety of regular phase separation patterns are formed, as shown in Fig. 6(d) for $t = 650$. Furthermore, we have also carried out a

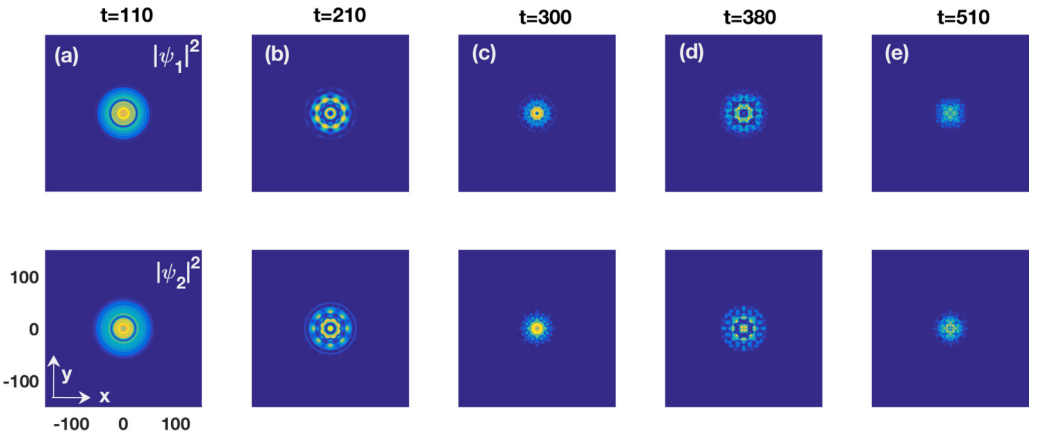

FIG. 8. The time evolutions of two black RDSs with resonant modulation frequency of the intercomponent interaction $\omega = 0.028$ for $t =$ (a) 110, (b) 210, (c) 300, (d) 380, and (e) 510 and for a larger computational box (typically, twice the size of Fig. 1). Other parameters are the same as those in Fig. 1.

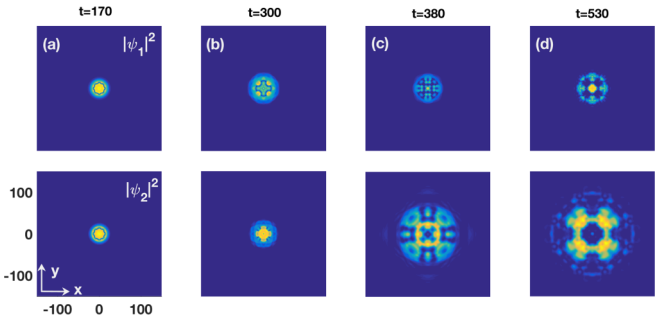

FIG. 9. The time evolutions of two black RDSs with modulation frequency $\omega = 0.01$ for $t =$ (a) 170, (b) 300, (c) 380, and (d) 530 and for a larger computational box (typically, twice the size of Fig. 1). Other parameters are the same as those in Fig. 1.

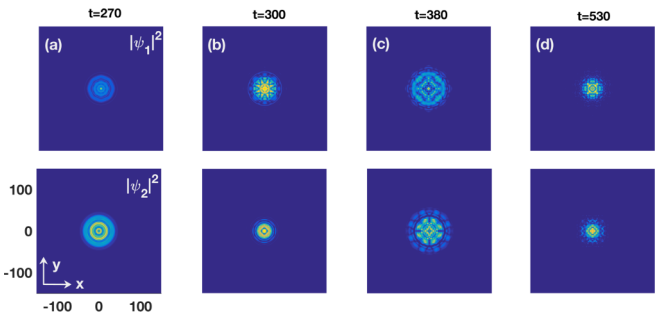

FIG. 10. The time evolutions of two black RDSs with modulation frequency $\omega = 0.05$ for $t =$ (a) 270, (b) 300, (c) 380, and (d) 530 and for a larger computational box (typically, twice the size of Fig. 1). Other parameters are the same as those in Fig. 1.

series of numerical experiments for two deep gray RDSs with different initial depths, which further confirmed the above conclusion.

To give a more clear description of dynamics of the RDSs, we plot the dependence of the lifetime of both black and deep gray RDSs on the modulation frequency, as shown in Fig. 7. It is easy to see that the lifetime of the gray RDS is longer than that of the black one for the same modulation frequency, which is consistent with our previous result. We note that this holds true for the case of modulation amplitude. In addition, for both black and gray RDSs cases, the lifetime of the RDS shows nonmonotonic dependence on the modulation parameters, and we attribute it to the complicated resonance phenomenon in the presence of the second component [26].

Finally, we also want to note that the various patterns obtained above always exhibit some symmetry, which is attributed to the circular symmetry of the initial RDSs, the numerical box, and the periodic boundary conditions, as discussed in Appendix A [51–53]. In the presence of periodic modulation of intercomponent interaction, the initially circular symmetry breaking gradually occurs with the formation of variously regular patterns. However, in the presence of a small (typically 1 or 5%) random perturbation (both in amplitude and phase at every point), new shallower RDSs appear and form a series of concentrically annular RDSs, then all the RDSs exhibit collective oscillation behavior until complete decay into radiation, during which no regular patterns are formed, as discussed in Appendix B. Since the time-splitting Fourier spectral method used in the present paper has second-order accuracy, we have performed the numerical study for the same parameter points through the fourth-order symplectic time integrator scheme, and the obtained results are qualitatively similar to those of the second-order one [54].

IV. CONCLUSIONS

In this paper, we have investigated the evolutions and pattern formation of two RDSs in a two-dimensional binary Bose-Einstein condensate with periodic modulation of the intercomponent interaction. Compared with the scalar condensate with fixed contact interaction, the lifetimes of both black and gray RDSs are largely extended in the presence of periodic modulation of the intercomponent interaction, and also show a strong dependence on the initial depths of the RDSs. It is found that new shallower RDSs are formed before snaking sets in, and their numbers and depths also perform collective oscillations with the initial black or gray one. We have also investigated the following decay dynamics of the system, showing complicated decaying dynamics. Depending on the modulation frequency of the intercomponent interaction and the initial depth of the RDS, the system exhibits a variety of decay profiles, such as vortex necklace, distorted octagon, vortex-antivortex ring, and cross.

Because of the much longer lifetime of the RDS, it provides a potential candidate for observing the long-time behavior of 2D dark solitons. Our results further enrich our knowledge on the dynamics of RDSs in ultracold atomic systems, and also other nonlinear systems, such as nonlinear optics, where the propagation of optical pulses can be described by a similar nonlinear Schrödinger equation.

ACKNOWLEDGMENTS

We would like to express our sincere thanks to Xinhua Hu for helpful discussions and Prof. Yongyong Cai for discussions on higher-order splitting approximations. This work

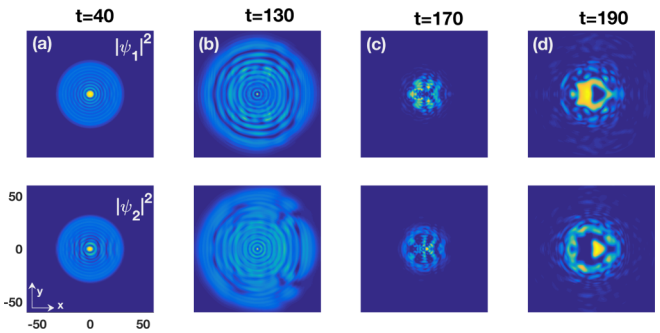

FIG. 11. The time evolutions of two black RDSs in the presence of a small (5%) random perturbation to both the amplitude and phase at every point, and for $t =$ (a) 40, (b) 130, (c) 170, and (d) 190. The modulation frequency of the intercomponent interaction $\omega = 0.028$. Other parameters are the same as those in Fig. 1.

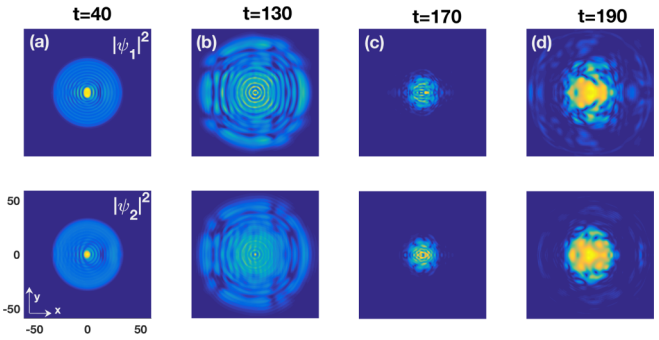

FIG. 12. The same as in Fig. 11 but for modulation frequency $\omega = 0.01$.

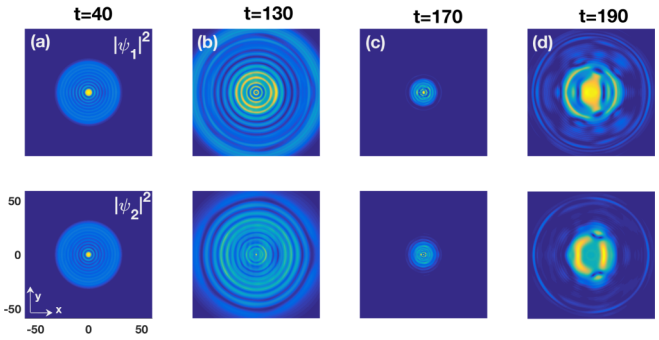

FIG. 13. The same as in Fig. 11 but for modulation frequency $\omega = 0.05$.

was supported by the National Natural Science Foundation of China under Grants No. 11775253, No. 11875010, No. 11504037, and No. 61504016; by the Natural Science Foundation of Hunan province under Grant No. 2018JJ3112; by the Zhejiang Provincial Natural Science Foundation of China under Grant No. LY17F050011; by the Youth Innovation Promotion Association of Chinese Academy of Sciences under Grant No. 2015334; and by the Chongqing Research Program of Basic Research and Frontier Technology under Grant No. cstc2014jcyjA50016.

APPENDIX A: THE EFFECT OF THE BOUNDARY CONDITIONS ON THE DYNAMICS

We consider the effect of the boundary condition on the dynamics of the system. As discussed previously, the numerical box and the periodic boundary conditions may have an important effect on the dynamics. The fact that the computational domain is squared introduces a symmetry in the system, which together with the initial RDSs and periodic boundary conditions explains why all the patterns formed during decay present this symmetry [51,53]. In Ref. [52], Vuong *et al.* have shown that the numerical method does not introduce spurious changes in the vortex due to the artificial square computational domain. We thus repeat the numerics with a larger computational box (typically, twice the size of the previous one). Figures 8–10 show the time evolutions of two black RDSs for a larger computational box, and for modulation frequencies $\omega = 0.028, 0.01,$ and 0.05, respectively. It is easy to see that the new results are consistent with our previous ones.

APPENDIX B: THE EFFECT OF THE RANDOM NOISE ON THE DYNAMICS

To check the effect of random nose, it is necessary to add a small amount of noise, both in amplitude and phase, to the initial condition. We have repeated the numerical study with the presence of a small (5%) random perturbation to both the amplitude and phase at every point, as shown in Figs. 11–13 for modulation frequencies $\omega = 0.028, 0.01,$ and 0.05, respectively. As shown in these figures, new shallower RDSs appear and form a series of concentrically annular RDSs, then all the RDSs exhibit collective oscillation behavior until complete decay into radiation, during which time no regular patterns are formed.

[1] T. L. Ho and V. B. Shenoy, Binary Mixtures of Bose Condensates of Alkali Atoms, Phys. Rev. Lett. **77**, 3276 (1996).
[2] B. D. Esry, C. H. Greene, J. P. Burke, and J. L. Bohn, Hartree-Fock Theory for Double Condensates, Phys. Rev. Lett. **78**, 3594 (1997).
[3] C. J. Myatt, E. A. Burt, R. W. Ghrist, E. A. Cornell, and C. E. Wieman, Production of Two Overlapping Bose-Einstein Condensates by Sympathetic Cooling, Phys. Rev. Lett. **78**, 586 (1997).
[4] H. Pu and N. P. Bigelow, Properties of Two-Species Bose Condensates, Phys. Rev. Lett. **80**, 1130 (1998).
[5] H. Pu and N. P. Bigelow, Collective Excitations, Metastability, and Nonlinear Response of a Trapped Two-Species Bose-Einstein Condensate, Phys. Rev. Lett. **80**, 1134 (1998).
[6] D. S. Hall, M. R. Matthews, J. R. Ensher, C. E. Wieman, and E. A. Cornell, Dynamics of Component Separation in a Binary Mixture of Bose-Einstein Condensates, Phys. Rev. Lett. **81**, 1539 (1998).
[7] G. Modugno, G. Ferrari, G. Roati, R. J. Brecha, A. Simoni, and M. Inguscio, Bose-einstein condensation of potassium atoms by sympathetic cooling, Science **294**, 1320 (2001).
[8] G. Thalhammer, G. Barontini, and L. D. Sarlo, Double Species Bose-Einstein Condensate with Tunable Interspecies Interactions, Phys. Rev. Lett. **100**, 210402 (2008).
[9] S. B. Papp, J. M. Pino, and C. E. Wieman, Tunable Miscibility in a Dual-Species Bose-Einstein Condensate, Phys. Rev. Lett. **101**, 040402 (2008).
[10] C. Becker, S. Stellmer, P. Soltan-Panahi, S. Dörscher, M. Baumert, E. M. Richter, J. Kronjäger, K. Bongs, and K. Sengstock, Oscillations and interactions of dark and dark-bright solitons in Bose-Einstein condensates, Nat. Phys. **4**, 496 (2008).
[11] D. J. Kaup and B. A. Malomed, Soliton trapping and daughter waves in the Manakov model, Phys. Rev. A **48**, 599 (1993).
[12] A. P. Sheppard and Y. S. Kivshar, Polarized dark solitons in isotropic Kerr media, Phys. Rev. E **55**, 4773 (1997).

[13] B. A. Malomed and R. S. Tasgal, Internal vibrations of a vector soliton in the coupled nonlinear Schrödinger equations, Phys. Rev. E **58**, 2564 (1998).

[14] T. H. Busch and J. R. Anglin, Dark-bright Solitons in Inhomogeneous Bose-Einstein Condensates, Phys. Rev. Lett. **87**, 010401 (2001).

[15] V. M. Pérez-García and J. B. Beitia, Symbiotic solitons in heteronuclear multicomponent Bose-Einstein condensates, Phys. Rev. A **72**, 033620 (2005).

[16] S. K. Adhikari, Bright solitons in coupled defocusing NLS equation supported by coupling: Application to Bose-Einstein condensation, Phys. Lett. A **346**, 179 (2005).

[17] X. Liu, H. Pu, B. Xiong, W. M. Liu, and J. Gong, Formation and transformation of vector solitons in two-species Bose-Einstein condensates with a tunable interaction, Phys. Rev. A **79**, 013423 (2009).

[18] X. F. Zhang, X. H. Hu, X. Liu, and W. M. Liu, Vector solitons in two-component Bose-Einstein condensates with tunable interactions and harmonic potential, Phys. Rev. A **79**, 033630 (2009).

[19] C. R. Cabrera, L. Tanzi, J. Sanz, B. Naylor, P. Thomas, P. Cheiney, and L. Tarruell, Quantum liquid droplets in a mixture of Bose-Einstein condensates, Science **359**, 301 (2018).

[20] S. Gautam and S. K. Adhikari, Self-trapped quantum balls in binary Bose-Einstein condensates, J. Phys. B **52**, 055302 (2019).

[21] Y. S. Kivshar and X. P. Yang, Ring dark solitons, Phys. Rev. E **50**, R40 (1994).

[22] A. Dreischuh, D. Neshev, G. G. Paulus, F. Grasbon, and H. Walther, Ring dark solitary waves: Experiment versus theory, Phys. Rev. E **66**, 066611 (2002).

[23] Y. V. Kartashov, V. A. Vysloukh, and L. Torner, Stable Ring-Profile Vortex Solitons in Bessel Optical Lattices, Phys. Rev. Lett. **94**, 043902 (2005).

[24] G. Theocharis, D. J. Frantzeskakis, P. G. Kevrekidis, B. A. Malomed, and Y. S. Kivshar, Ring Dark Solitons and Vortex Necklaces in Bose-Einstein Condensates, Phys. Rev. Lett. **90**, 120403 (2003).

[25] S. J. Yang, Q. S. Wu, S. N. Zhang, S. Feng, W. Guo, Y. C. Wen, and Y. Yu, Generating ring dark solitons in an evolving Bose-Einstein condensate, Phys. Rev. A **76**, 063606 (2007).

[26] X. H. Hu, X. F. Zhang, D. Zhao, H. G. Luo, and W. M. Liu, Dynamics and modulation of ring dark solitons in two-dimensional Bose-Einstein condensates with tunable interaction, Phys. Rev. A **79**, 023619 (2009).

[27] S. W. Song, D. S. Wang, H. Wang, and W. M. Liu, Generation of ring dark solitons by phase engineering and their oscillations in spin-1 Bose-Einstein condensates, Phys. Rev. A **85**, 063617 (2012).

[28] L. A. Toikka and K. A. Suominen, Snake instability of ring dark solitons in toroidally trapped Bose-Einstein condensates, Phys. Rev. A **87**, 043601 (2013).

[29] S. Donadello, S. Serafini, M. Tylutki, L. P. Pitaevskii, F. Dalfovo, G. Lamporesi, and G. Ferrari, Observation of Solitonic Vortices in Bose-Einstein Condensates, Phys. Rev. Lett. **113**, 065302 (2014).

[30] T. Kaneda and H. Saito, Dynamics of a vortex dipole across a magnetic phase boundary in a spinor Bose-Einstein condensate, Phys. Rev. A **90**, 053632 (2014).

[31] W. Wang, P. G. Kevrekidis, R. Carretero-González, D. J. Frantzeskakis, T. J. Kaper, and M. Ma, Stabilization of ring dark solitons in Bose-Einstein condensates, Phys. Rev. A **92**, 033611 (2015).

[32] L. X. Wang, C. Q. Dai, L. Wen, T. Liu, H. F. Jiang, H. Saito, S. G. Zhang, and X. F. Zhang, Dynamics of vortices followed by the collapse of ring dark solitons in a two-component Bose-Einstein condensate, Phys. Rev. A **97**, 063607 (2018).

[33] S. Inouye, M. R. Andrews, J. Stenger, H. J. Miesner, D. M. Stamper-Kurn, and W. Ketterle, Observation of Feshbach resonances in a Bose-Einstein condensate, Nature (London) **392**, 151 (1998).

[34] J. L. Roberts, N. R. Claussen, J. P. Burke, Jr, C. H. Greene, E. A. Cornell, and C. E. Wieman, Resonant Magnetic Field Control of Elastic Scattering in Cold ^{85}Rb, Phys. Rev. Lett. **81**, 5109 (1998).

[35] E. A. Donley, N. R. Claussen, S. L. Cornish, J. L. Roberts, E. A. Cornell, and C. E. Wieman, Dynamics of collapsing and exploding Bose-Einstein condensates, Nature (London) **412**, 295 (2001).

[36] C. Chin, R. Grimm, P. Julienne, and E. Tiesinga, Feshbach resonances in ultracold gases, Rev. Mod. Phys. **82**, 1225 (2010).

[37] T. Chen and B. Yan, Characterization of stimulated excitations in a driven Bose-Einstein condensate, Phys. Rev. A **98**, 063615 (2018).

[38] A. Griffin, Conserving and gapless approximations for an inhomogeneous Bose gas at finite temperatures, Phys. Rev. B **53**, 9341 (1996).

[39] F. Kh. Abdullaev, J. G. Caputo, R. A. Kraenkel, and B. A. Malomed, Controlling collapse in Bose-Einstein condensates by temporal modulation of the scattering length, Phys. Rev. A **67**, 013605 (2003).

[40] S. K. Adhikari, Stabilization of bright solitons and vortex solitons in a trapless three-dimensional Bose-Einstein condensate by temporal modulation of the scattering length, Phys. Rev. A **69**, 063613 (2004).

[41] L. Salasnich, A. Parola, and L. Reatto, Effective wave equations for the dynamics of cigar-shaped and disk-shaped Bose condensates, Phys. Rev. A **65**, 043614 (2002).

[42] W. H. Press, S. A. Teukolsky, W. T. Vetterling, and B. P. Flannery, *Numerical Recipes in Fortran 77* (Cambridge University, Cambridge, England, 1992).

[43] K. Kasamatsu, M. Tsubota, and M. Ueda, Nonlinear dynamics of vortex lattice formation in a rotating Bose-Einstein condensate, Phys. Rev. A **67**, 033610 (2003).

[44] W. Z. Bao, D. Jaksch, and P. Markowich, Numerical solution of the Gross-Pitaevskii equation for Bose-Einstein condensation, J. Comput. Phys. **187**, 318 (2003).

[45] S. Burger, K. Bongs, S. Dettmer, W. Ertmer, K. Sengstock, A. Sanpera, G. V. Shlyapnikov, and M. Lewenstein, Dark Solitons in Bose-Einstein Condensates, Phys. Rev. Lett. **83**, 5198 (1999).

[46] K. C. Wright, L. S. Leslie, A. Hansen, and N. P. Bigelow, Sculpting the Vortex State of a Spinor BEC, Phys. Rev. Lett. **102**, 030405 (2009).

[47] S. K. Adhikari, Stable and mobile two-dimensional dipolar ring-dark-in-bright Bose-Einstein condensate soliton, Laser Phys. Lett. **13**, 035502 (2016).

[48] V. V. Konotop and L. Pitaevskii, Landau Dynamics of a Grey Soliton in a Trapped Condensate, Phys. Rev. Lett. **93**, 240403 (2004).

[49] C. J. Pethick and H. Smith, *Bose-Einstein Condensation in Dilute Gases* (Cambridge University, Cambridge, England, 2002).

[50] L. Pitaevskii and S. Stringari, *Bose-Einstein Condensation* (Oxford University, New York, 2003).

[51] A. Ferrando, M. Zacarés, M.-A. García-March, J. A. Monsoriu, and P. F. de Córdoba, Vortex Transmutation, Phys. Rev. Lett. **95**, 123901 (2005).

[52] L. T. Vuong, T. D. Grow, A. Ishaaya, A. L. Gaeta, G. W. 't Hooft, E. R. Eliel, and G. Fibich, Collapse of Optical Vortices, Phys. Rev. Lett. **96**, 133901 (2006).

[53] V. M. Pérez-García, M.-A. García-March, and A. Ferrando, Symmetry-assisted vorticity control in Bose-Einstein condensates, Phys. Rev. A **75**, 033618 (2007).

[54] W. Bao and J. Shen, A fourth-order time-splitting Laguerre-Hermite pseudospectral method for Bose-Einstein condensates, SIAM J. Sci. Comput. **26**, 2010 (2005).